

Forschungszentrum Karlsruhe

in der Helmholtz -Gemeinschaft

Wissenschaftliche Berichte

FZKA 6778

**Magnetohydrodynamic flow
in the European SCLL blanket concept**

L. Bühler and L. Giancarli *

Institut für Kern - und Energietechnik
Programm Kernfusion

* CEA, Saclay, France

Impressum der Print-Ausgabe:

**Als Manuskript gedruckt
Für diesen Bericht behalten wir uns alle Rechte vor**

**Forschungszentrum Karlsruhe GmbH
Postfach 3640, 76021 Karlsruhe**

**Mitglied der Hermann von Helmholtz-Gemeinschaft
Deutscher Forschungszentren (HGF)**

ISSN 0947-8620

Magnetohydrodynamic flow in the European SCLL blanket

Abstract

The pressure drop and flow patterns of fully developed liquid metal flow in a typical geometry of the European SCLL blanket exposed to a uniform magnetic field has been evaluated. The calculations for an outboard blanket in a field of $B_0 = 4$ T show that the pressure gradient in ducts made by electrically insulating walls is about $\nabla p = 0.0567$ MPa/m at maximum velocities of $v_0 = 4.5$ m/s in the annular gap, which seems to be acceptable. The pressure drop in the central duct is very small so that the total pressure drop is mainly created in the annular gap flow. Values for the top and inboard blanket are estimated by extrapolation.

It is found that the core velocity profiles along the first wall exhibit a decrease when approaching the walls, which divide the annular gap into a number of sub channels. This "periodic" velocity distribution creates non-uniform temperature distributions along the first wall, a fact that has to be considered in future stress analyses.

Magnetohydrodynamische Strömungen im Europäischen SCLL Blanket

Zusammenfassung

In diesem Bericht werden Ergebnisse zu Druckverlust und Geschwindigkeitsverteilung eingelaufener Flüssigmetall-Strömungen im Europäischen SCLL Blanket vorgestellt. Berechnungen für ein Outboard-Blanket in einem konstanten Magnetfeld von $B_0 = 4$ T ergeben akzeptable Druckverluste von $\nabla p = 0.0567$ MPa/m in den elektrisch isolierten Spalten bei Strömungsgeschwindigkeiten von $v_0 = 4.5$ m/s. Der Druckverlust im zentralen Kanal ist viel geringer, so dass der Gesamtdruckabfall sich hauptsächlich aus der Spaltströmung ergibt. Werte für Top- und Inboard-Blanket werden durch eine Extrapolation abgeschätzt.

Die Geschwindigkeitsprofile zeigen einen Abfall in der Nähe der Wände, die den kreisförmigen Ringspalt in mehrere Unterkanäle aufteilen. Diese "periodische" Geschwindigkeitsverteilung hat Temperaturschwankungen entlang der ersten Wand zur Folge, was bei zukünftigen mechanischen Spannungsrechnungen berücksichtigt werden sollte.

Magnetohydrodynamic flow in the European SCLL blanket

Contents

1	Introduction	1
2	Formulation	4
2.1	Governing equations	4
2.2	Material properties	7
3	Results for design 1	8
3.1	Annular sub channels	8
3.1.1	Duct D1	9
3.1.2	Ducts D2 and D3	11
3.1.3	Ducts D4 and D5	15
3.2	The whole annular region	16
3.3	Central duct	19
4	Results for design 2	20
4.1	Annular sub channels	20
5	Conclusions	23

1 Introduction

Within the framework of the European Power Plant Conceptual Studies, launched in January 2000, the most advanced reactor model is based on a Self-Cooled Lithium-Lead (SCLL) blanket concept. This reactor is associated with the largest attractiveness and at the same time with the largest development risk. It is based on the use of SiC/SiC structures which allow high coolant temperature, and show very low short term activation and afterheat levels. Associated with the use of Pb-17Li as coolant, breeder, and coolant tritium carrier, this system allows to achieve high plant efficiency while reactor passive safety becomes possible by minimizing the available energy sources within the vacuum vessel.

The proposed SCLL design is based on the most attractive features of the previously studied TAURO and ARIES-AT blanket concepts. A radial cut of the reactor is shown in Fig. 1 and a blanket segment is shown in Figs. 2 and 3 for the equatorial plane. The blanket is essentially formed by two concentric boxes where the cold Pb-17Li flows in at high velocity in the outer gap and flows out at low velocity through an inner channel. The interaction of the electrically conducting coolant with the magnetic field confining the fusion plasma causes magnetohydrodynamic (MHD) pressure drops and flow pattern that differ from hydrodynamic ones. The pressure drop is minimized because of the relatively low electrical conductivity of the SiC/SiC structure material.

MHD flows in the TAURO blanket had been studied previously (Bühler (1999), Bühler (2001)). Since the SCLL blanket has some common features like curved first wall, relatively thin gap behind the first wall etc. one could think that those results should apply for the present SCLL design as well. A major effect that had been observed during the TAURO analysis was the fact that even through the poorly conducting dividing wall an electrical coupling between the annular flow and the flow in the central pipe was possible with the consequence of partly reversed flow in the gap that could cause closed recirculation loops. This behavior seems to be less severe here because of several reasons. One reason is that the dividing wall here is thicker than for TAURO providing therefore higher electric resistance for electric currents crossing the wall. Another reason is that in the current SCLL design the annular gap is divided into a number of sub channels, a fact that may prevent the flow from establishing large recirculation loops, which have dimensions of the size of the whole annular gap. The gap width in SCLL is much smaller than that used in TAURO. The velocity in the gap is therefore by more than an order of magnitude larger than that in the central channel. If a slight coupling may occur we could rather expect that the gap drives a secondary motion in the inner channel with less severe consequences for heat or mass transfer. For all these reasons we treat the walls as perfect insulators during this first step of MHD analysis. A confirmation of this assumption by experiments would be desirable.

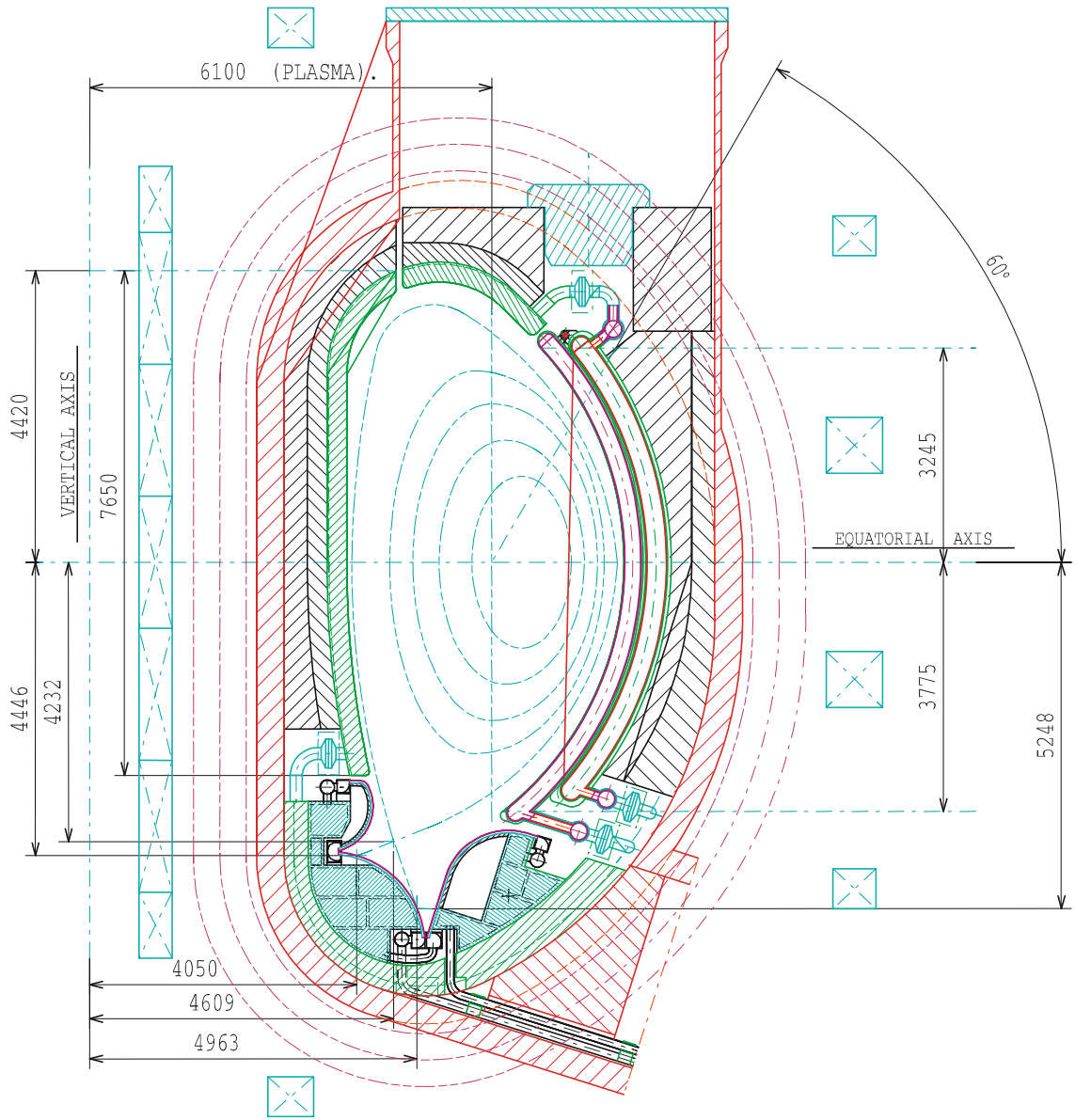


Figure 1: SCLL reactor design (Enderlé et al. (2002)). Main plasma chamber dimensions. The length of the outboard, top, and inboard blanket is about 7.8 m, 2.2 m, and 7.7 m, respectively.

2 Formulation

2.1 Governing equations

The liquid metal with density ρ , kinematic viscosity ν and electric conductivity σ flows with typical velocity v_0 in the SCLL blanket, exposed to a uniform externally applied toroidal magnetic field $B_0\hat{\mathbf{z}}$. A typical length scale for the flow near the first wall is the gap width L . The proper scale for the flow in the central channels would be the half width of the duct measured along magnetic field lines. The flow is governed by dimensionless conservation equations for momentum, mass, and charge, equation

$$\frac{1}{N} \left[\frac{\partial}{\partial t} + (\mathbf{v} \cdot \nabla) \right] \mathbf{v} = -\nabla p + \frac{1}{Ha^2} \nabla^2 \mathbf{v} + \mathbf{j} \times \mathbf{B}, \quad (1)$$

$$\nabla \cdot \mathbf{v} = 0, \quad (2)$$

$$\nabla \cdot \mathbf{j} = 0, \quad (3)$$

and by Ohm's law

$$\mathbf{j} = -\nabla\phi + \mathbf{v} \times \mathbf{B}. \quad (4)$$

Here, \mathbf{v} , \mathbf{B} , \mathbf{j} , p , ϕ stand for velocity, applied magnetic field, current density, pressure, and electric potential, scaled by reference values v_0 , the magnitude of the applied magnetic induction B_0 , $j_0 = \sigma v_0 B_0$, $p_0 = L\sigma v_0 B_0^2$, and $\phi_0 = Lv_0 B_0$, respectively.

This set of equations (1)-(4) has to be solved for adequate kinematic and electrical boundary conditions at the fluid-wall interface Γ . The kinematic and electric boundary conditions at an insulating surface are

$$\mathbf{v} = 0, \text{ and } \mathbf{j} \cdot \mathbf{n} = 0 \text{ at } \Gamma. \quad (5)$$

The two dimensionless groups are the interaction parameter

$$N = \frac{\sigma L B_0^2}{\rho v_0} \quad (6)$$

and the Hartmann number

$$Ha = LB_0 \sqrt{\frac{\sigma}{\rho \nu}}. \quad (7)$$

The interaction parameter and the square of the Hartmann number give the ratio of electromagnetic to inertia forces and electromagnetic to viscous forces, respectively. In the following we restrict the analysis to stationary, fully established conditions for which the left-hand side of (1) vanishes identically. Alternatively we could also deal with weakly inertial three-dimensional flows in strong fields for which the interaction parameter is large, i.e. $N \gg 1$. Moreover, for all application in fusion blankets the Hartmann number is very high, $Ha \gg 1$, so that in the *core* viscous forces are negligible in comparison with electromagnetic forces which balance the pressure gradient in this regime. Viscosity plays a role only in the thin viscous boundary layers near the walls which provide a path for current closure. These layers in which the magnetic field has a normal component are called the Hartmann layers and they scale in thickness as

$\delta \sim Ha^{-1}$, resulting in relatively high resistance for the electric circuit. The electric currents are small and the nondimensional pressure drop scales in insulating ducts as

$$\nabla p \sim Ha^{-1}. \quad (8)$$

The governing equations are solved using a numerical code based on asymptotic techniques (see Bühler (1994)). This code solves the inviscid inertialess problem for the three-dimensional flows in the core but accounts for viscous effects in thin boundary layers along the walls. Since viscosity acts only within the layers, the boundary conditions that apply to the flow in the core modify to

$$\mathbf{v} \cdot \mathbf{n} = 0, \text{ and } \mathbf{j} \cdot \mathbf{n} = -\nabla \cdot \int \mathbf{j}_{\delta,t} dn \text{ at } \Gamma. \quad (9)$$

Here $\mathbf{j}_{\delta,t}$ are the viscous corrections to the currents in the layers, in a plane tangential to the wall. In a further step the currents in the layer are expressed using the electric potential. It is well known that the potential does not change at leading order across the layer so that the potential in the layer is the same as that of the inviscid solution in the core at Γ (see e.g. Moreau (1990), Müller and Bühler (2001)). After integration of (9) and using (5) at the wall, the final electrical condition for the core variables reads

$$\mathbf{j} \cdot \mathbf{n} = \nabla_t \cdot (\delta \nabla_t \phi) \text{ at } \Gamma, \quad (10)$$

where $\delta = (\mathbf{B} \cdot \mathbf{n} Ha)^{-1}$ is the local thickness of the viscous layer and ∇_t represents the tangential components of the gradient vector. After the flow in the core is determined it is possible to reconstruct the viscous profiles of all variables within the layers.

The numerical code uses a special type of boundary fitted coordinates. In the core one coordinate is chosen parallel to the applied magnetic field, i.e. parallel to $\hat{\mathbf{z}}$. The details of a coordinate transformation such as

$$\mathbf{x} = \bar{\mathbf{x}}(u^1, u^2) + h(u^1, u^2) u^3 \hat{\mathbf{z}} \quad (11)$$

are shown in Fig. 4. Any magnetic field line that penetrates the fluid-wall interface Γ twice contains the point $\bar{\mathbf{x}}$, which divides the distance between the two penetration points into two parts of length h . The coordinate $\bar{\mathbf{x}}$ and the half height h are functions of the two transverse and axial coordinates u^1 and u^2 only. The transformation maps the arbitrary fluid region to a standard volume $0 < u^1 < 1$, $0 < u^2 < 1$, $-1 < u^3 < 1$, where Γ is defined as $u^3 = -1$ and $u^3 = 1$, at the *bottom* and at the *top*, respectively. The only restriction that arises from the use of this transformation is that walls which are perfectly aligned with the magnetic field are excluded from the analysis. Further details about the analysis or the numerical method have been reported by Bühler (1994) and the latter reference describes also methods how to deal with parallel walls.

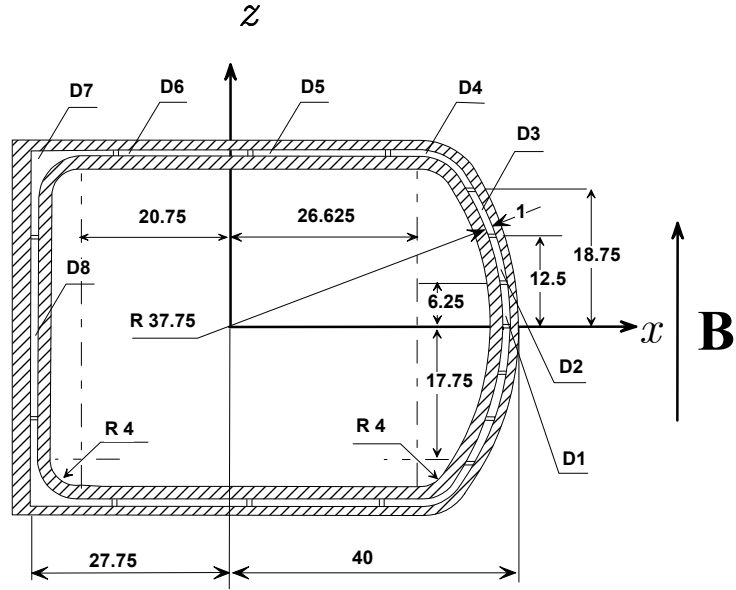


Figure 3: Sketch of the front part of the SCLL blanket. All dimensions are normalized with the gap width $L = 4$ mm near the first wall. Ducts forming the gap are numbered as D1, D2, etc.

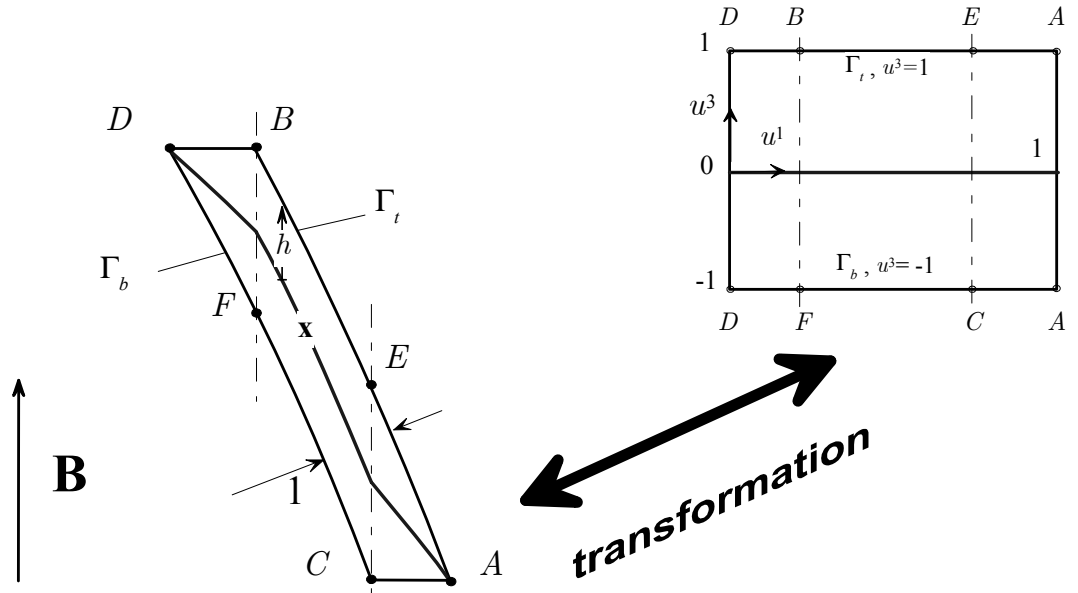


Figure 4: Details of coordinates for duct D3. The corners are denoted by A, B, C, D ; internal layers spread from the corners B and C into the fluid separating the interior of the channel into three cores. The points B and F , and C and E , belong to the same internal layer, respectively

2.2 Material properties

The liquid $Li(17)Pb(83)$ in the blanket will flow at temperatures $700^\circ\text{C} < T < 1100^\circ\text{C}$. To the authors' knowledge there exists currently no complete data base that covers this high temperature range. The data proposed by Jauch, Karcher, Schulz and Haase (1986) is validated in the temperature ranges shown in Tab 1. This data agrees well with polynomial fittings presented by Malang and Tillack (1995) in their range of validity. Polynomial fits cannot be extended beyond measured data points. Here, the density and the electric resistivity vary linearly with temperature and the viscosity $\eta = \rho\nu$ is derived from an Arrhenius law. The latter facts suggest that extrapolations to higher values of temperature are possible and Jauch et al. (1986) expect reasonable values of data at least up to 1250 K. Values for electric conductivity are derived from the data shown above as

$$\sigma = \frac{1}{\rho_{el}}. \quad (12)$$

Table 1: Properties of LiPb

density	ρ	=	$10.45 (1 - 161 \cdot 10^{-6}T/\text{K})$	kg/m^3	$508 \text{ K} < T < 625 \text{ K}$
electric resistivity	$\rho_{el} = \sigma^{-1}$	=	$(102.3 + 0.0426T/\text{K}) \cdot 10^{-8}$	$\Omega \text{ m}$	$508 \text{ K} < T < 933 \text{ K}$
dynamic viscosity	$\eta = \rho\nu$	=	$0.187 \cdot 10^{-3} \exp\left(\frac{11640}{8.314T/\text{K}}\right)$	Pa s	$508 \text{ K} < T < 933 \text{ K}$

3 Results for design 1

3.1 Annular sub channels

The analysis is based on the input data that has been made available to the author by L. Giancarli. More details will be published in future papers, e.g. Giancarli, Bühler, U. Fischer and, Maisonnier, Poitevin, Szczepanski and Ward (2003). The values for the magnetic field can be found in Fig. 5. From the figure one can roughly estimate the magnitude of toroidal magnetic field $B_0 = 4, 6, 8$ T for the outboard, the top, and the inboard blanket, respectively. As a first step the fully established MHD flow in the blanket is evaluated, assuming infinitely long ducts of uniform cross sections in a uniform magnetic field. The pressure drop is given for the outboard blanket, i.e. for a magnetic field of $B_0 = 4$ T. With fluid data at temperature near 900°C and a characteristic length $L = 0.004$ m the Hartmann number evaluates to $Ha \approx 520$. The nondimensional pressure drop scales as $\nabla p \sim Ha^{-1}$, where the magnitude of the magnetic field enters the relation through the Hartmann number. Assuming similar cross sections it is possible to give estimates also for the pressure drop in the top and inboard blanket using the known scaling laws. A detailed analysis using varying cross section and spatially varying magnetic fields is in principle possible and foreseen for future analyses.

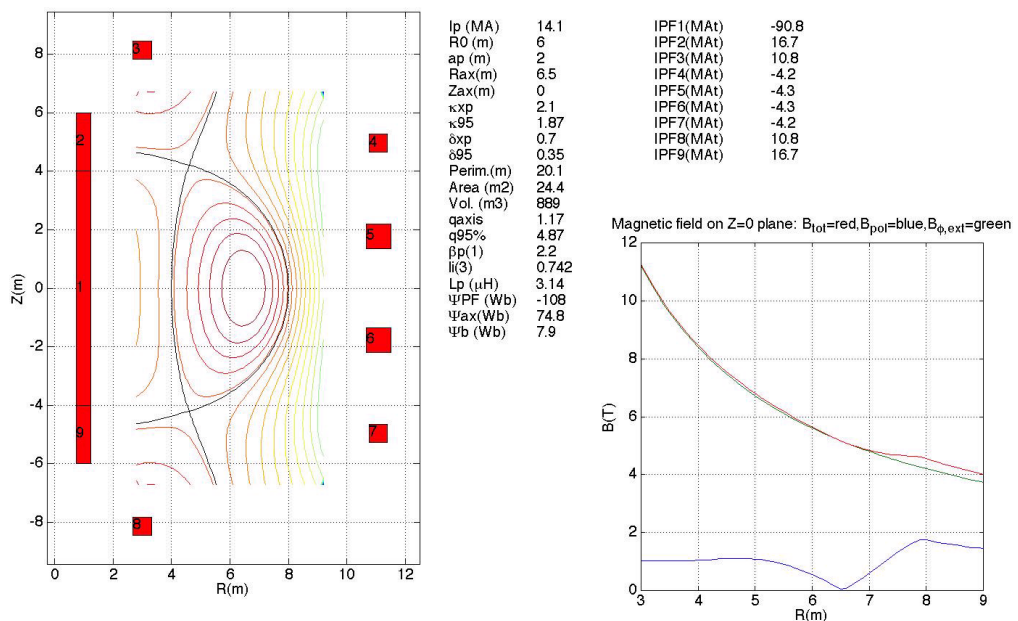


Figure 5: Distribution of the toroidal magnetic field.

3.1.1 Duct D1

Let us start the description of results for the duct D1. The calculation was done by assuming a number of 60 grid points in the x - direction (radial). Checks with higher resolution proved that the accuracy is good enough, i.e. the pressure drop is correct with an error less than $1^\circ/\infty$. The direction along magnetic field lines is resolved analytically by the asymptotic approach. The number of points forming the grid in this direction is chosen in order to give convenient figures for data presentation. The number of points is irrelevant for the computation.

Colored contours of axial velocity are shown in Fig. 6. The figure shows that isolines of velocity are preferentially aligned with the applied magnetic field along the z -direction. This observation is in accordance with the well known result that the velocity depends roughly on the extension of the insulating duct measured along magnetic field lines. This means that high velocities are expected between the two internal layers that spread into the fluid from the points B and C . The width of the duct measured along field lines decreases monotonically when we move along the first wall from the position B to A . As a consequence the core velocity near the first wall decreases also monotonically to zero when approaching A . This fact should be taken into account during a heat transfer analysis for the blanket. For the same reasons as just mentioned the velocity decreases also when we approach the point D . However, since this point does not receive the highest heat flux this is not considered as a critical issue.

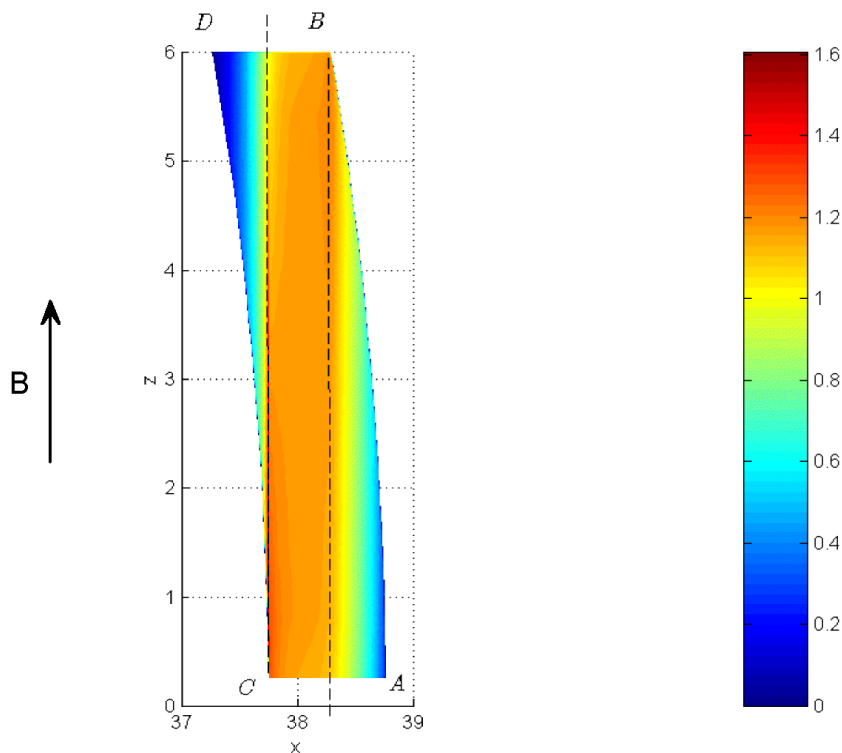


Figure 6: Colored contours of velocity in duct D1

The same data is shown in addition in Figs. 7 and 8 as a perspective view from the inner duct and from the first wall, respectively to give the reader the three-dimensional impression of the flow. In these figures the thin Hartmann layers are visible and the structure of the flow in both outer cores becomes better visible. Especially when we approach the internal layer near C the velocity increases strongly. This result is caused by the inner wall, which becomes aligned with the magnetic field at the point C . The asymptotic methods used here give discontinuous profiles of velocity caused by the discontinuous slope of the wall at corners, here at the point C . These jumps of velocity are smoothly matched by viscosity in the internal layer within a thickness of the order $\delta_p \sim Ha^{-1/2}$. Since these layers do not carry an order one flow rate they do not affect the pressure drop at the leading order and they are therefore not considered in more detail. The nondimensional pressure drop in duct D1 evaluates as $\nabla p_1 = 0.0777 \cdot 10^{-2}$.

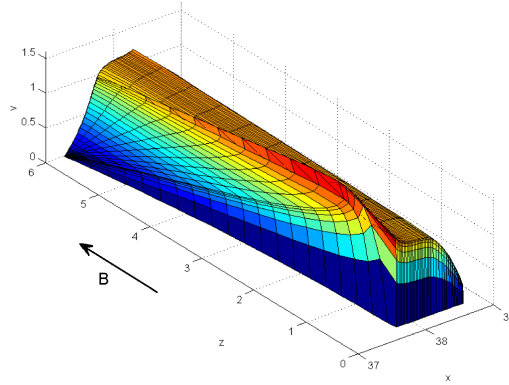


Figure 7: Perspective view from inside on the velocity profile in duct D1

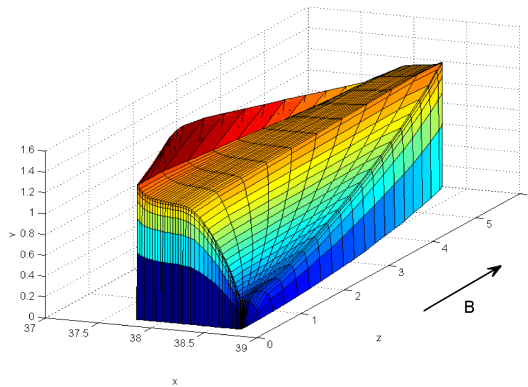


Figure 8: Perspective view from the first wall on the velocity profile in duct D1

3.1.2 Ducts D2 and D3

The results for velocity in ducts D2 and D3 are quite similar. The results are shown in a sequence of figures, Figs. 9-14. However, the regions of reduced velocity along the first wall is smaller for these ducts. Nevertheless, the velocity reduces to zero, not only in thin boundary layers but within the whole outer cores when we approach the points *A* or *D*. The core velocity is now continuous across internal parallel layers. This is different to the previous result for D1 and it is explained by the fact that now the wall does not become aligned with the magnetic field.

Duct D2

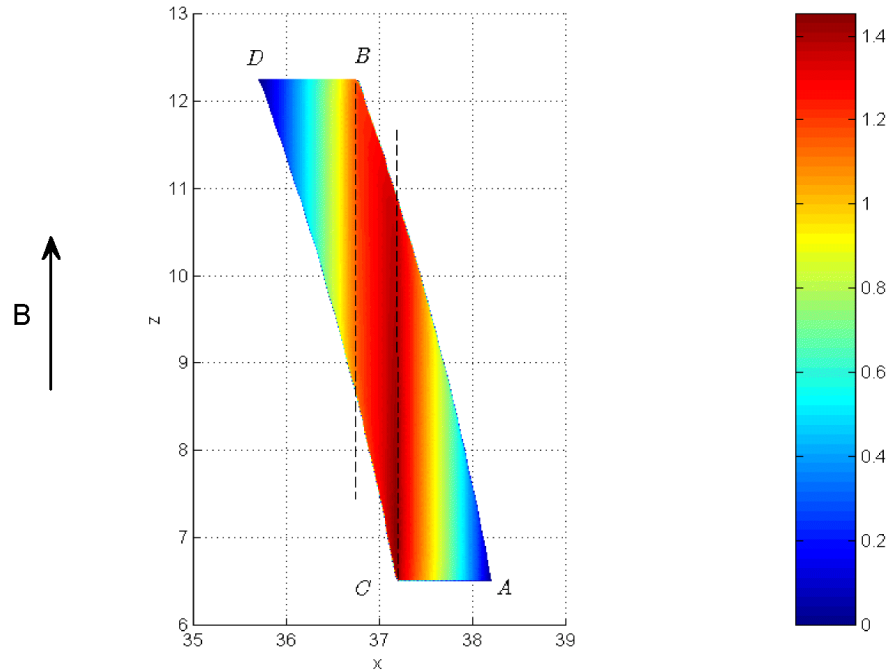


Figure 9: Colored contours of velocity in duct D2

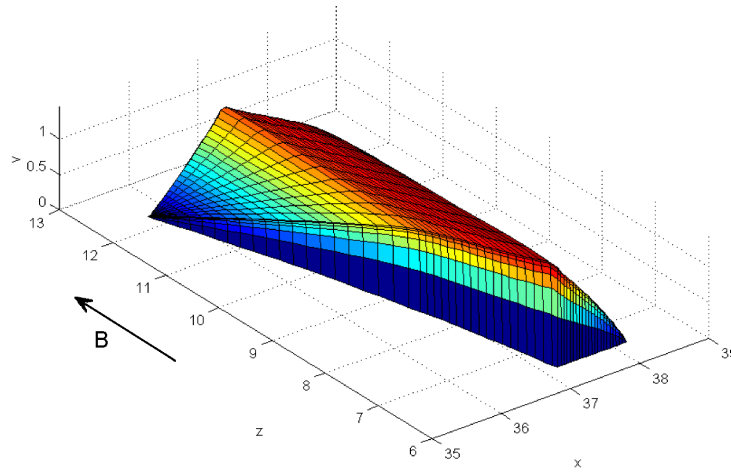


Figure 10: Perspective view from inside on the velocity profile in duct D2

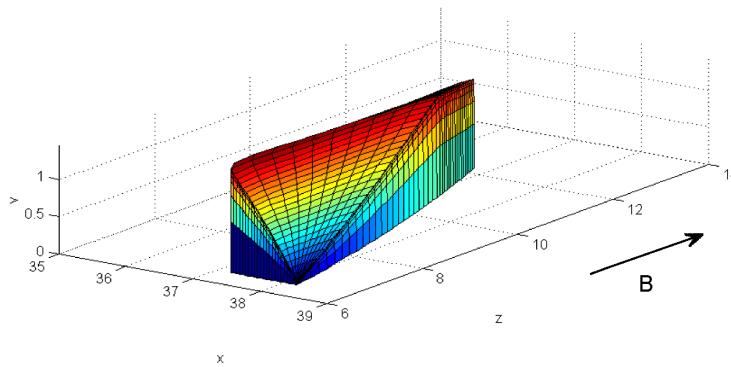


Figure 11: Perspective view from the first wall on the velocity profile in duct D2

Duct D3

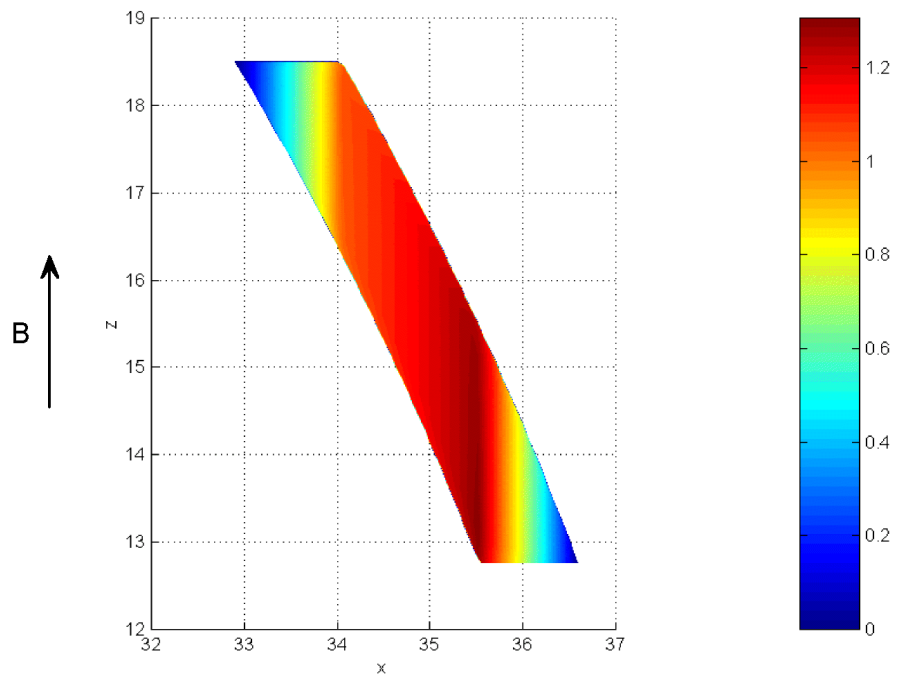


Figure 12: Colored contours of velocity in duct D3

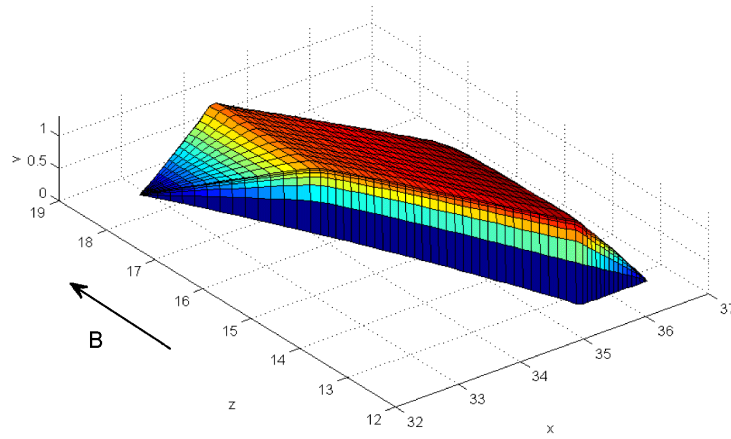


Figure 13: Perspective view from inside on the velocity profile in duct D3

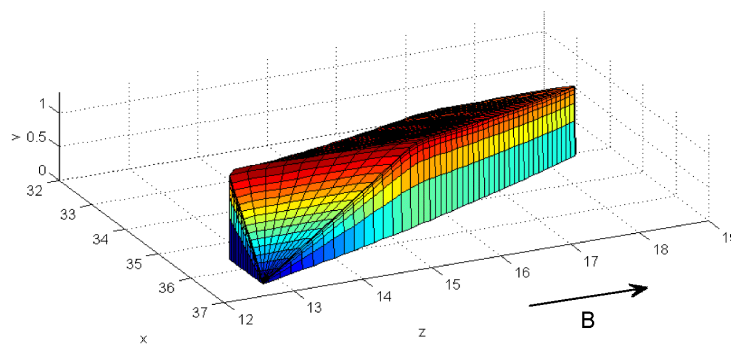


Figure 14: Perspective view from the first wall on the velocity profile in duct D3

3.1.3 Ducts D4 and D5

The flow in Duct D4, shown in Fig. 15, is a combination of the flow in ducts D1-D3 and the well known result for rectangular duct flow (see also Fig. 16). In the latter one the velocity profile is uniform in the whole core, except in the thin viscous boundary layers near the wall. When we approach the arcuate walls the extension of the duct along field lines increases and so does the velocity. Near point *A* we observe again a decrease of velocity.

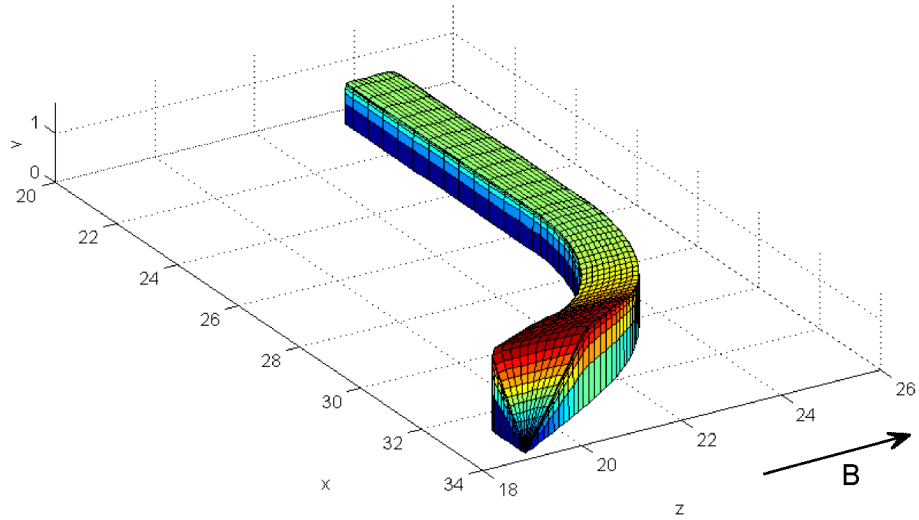


Figure 15: Perspective view on the velocity profile in duct D4

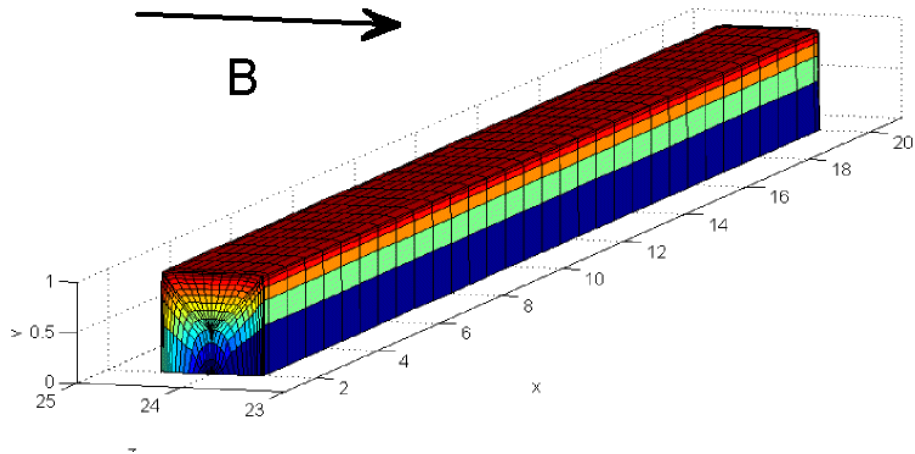


Figure 16: Perspective view on the velocity profile in duct D5

3.2 The whole annular region

To get an overall impression of the flow we may summarize all results in Fig. 17. For this figure it has been assumed that the average velocity in each sub channel is the same. To achieve this it would be necessary to adjust or control the flow by external means, which could become a difficult task since the pressure drops in all sub channels are different. The pressure drops are summarized in Tab. 2.

Table 2: Pressure gradient in sub channels for equal flow rates

Duct	∇p	v_0	∇p (MPa/m)	v_0 (m/s)
D1	0.000777	1.0	0.0343	4.2
D2	0.001219	1.0	0.0538	4.2
D3	0.001811	1.0	0.0799	4.2
D4	0.003197	1.0	0.1411	4.2
D5	0.003829	1.0	0.1689	4.2

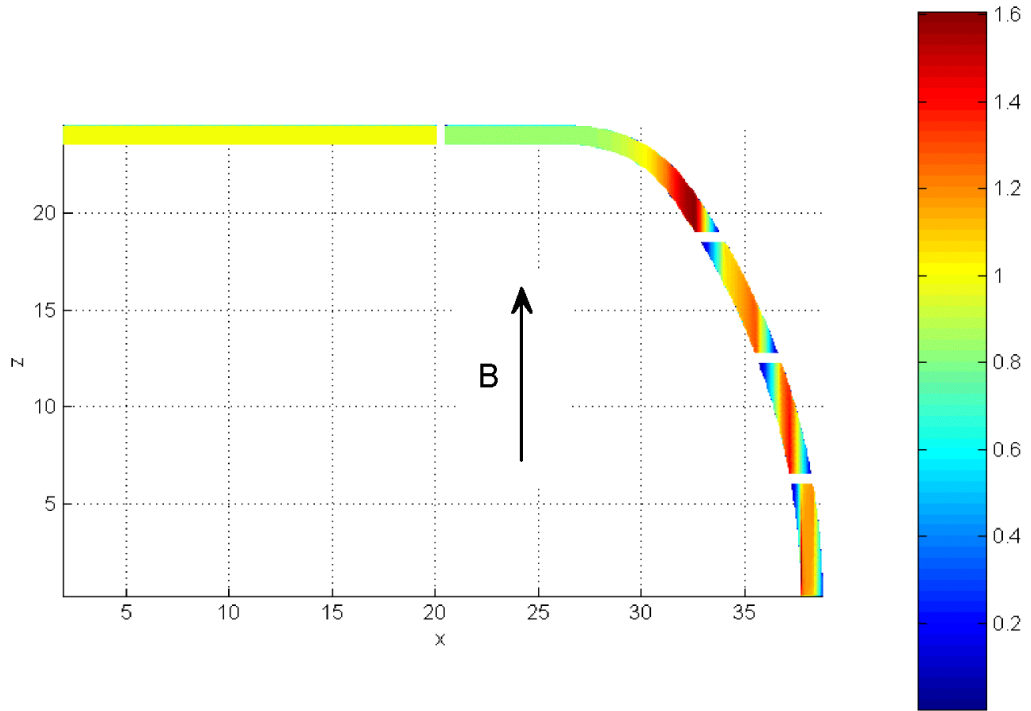


Figure 17: Colored contours of velocity in sub channels D1-D5 for an overview. Equal average velocities in all sub channels.

More realistically we could connect all ducts to the same "pressure reservoirs", say to the same supplying line and assume equal pressure drops due to distribution. Same pressure drops in all ducts cause now unequal flow rates or the average velocities. This influence on the flow rates is shown in Tab. 3 and in Fig. 18.

Table 3: Average velocities in sub channels for equal pressure drop

Duct	∇p	v_0	∇p (MPa/m)	v_0 (m/s)
D1	0.003829	4.905	0.1689	20.60
D2	0.003829	3.139	0.1689	13.18
D3	0.003829	2.114	0.1689	8.87
D4	0.003829	1.198	0.1689	5.03
D5	0.003829	1.000	0.1689	4.2

As a result we observe that the average velocity increases by a factor of 5 when we approach the center of the first wall in the blanket module. Nevertheless, we must keep in mind that regions of reduced velocities near the points *A* are still present. On the other hand a velocity of 20 m/s for a fluid like PbLi seems to be unrealistic for engineering applications. It is possible to reduce the large differences in velocity and to achieve more homogeneous velocity distributions if we change the size of the channels, i.e. their dimensions measured along field lines, by using a variable gap size or changing the distance between walls dividing the annular region into a number of sub channels.

So far, no calculations have been made for the flows in the ducts D7 and D8. The flow in D7 will be qualitatively similar to that in duct D4. It will be composed by a part that has Hartmann-type profiles in regions where the extension along field lines is uniform. In the other region we expect that the velocity increases strongly as the dimension of the duct measured along field lines. As a consequence we expect high velocities in the rear gap so that perhaps, most flow is carried here instead of being carried in the first wall ducts D1-D4. This problem can be solved easily by dividing the rear gap into a larger number of sub channels.

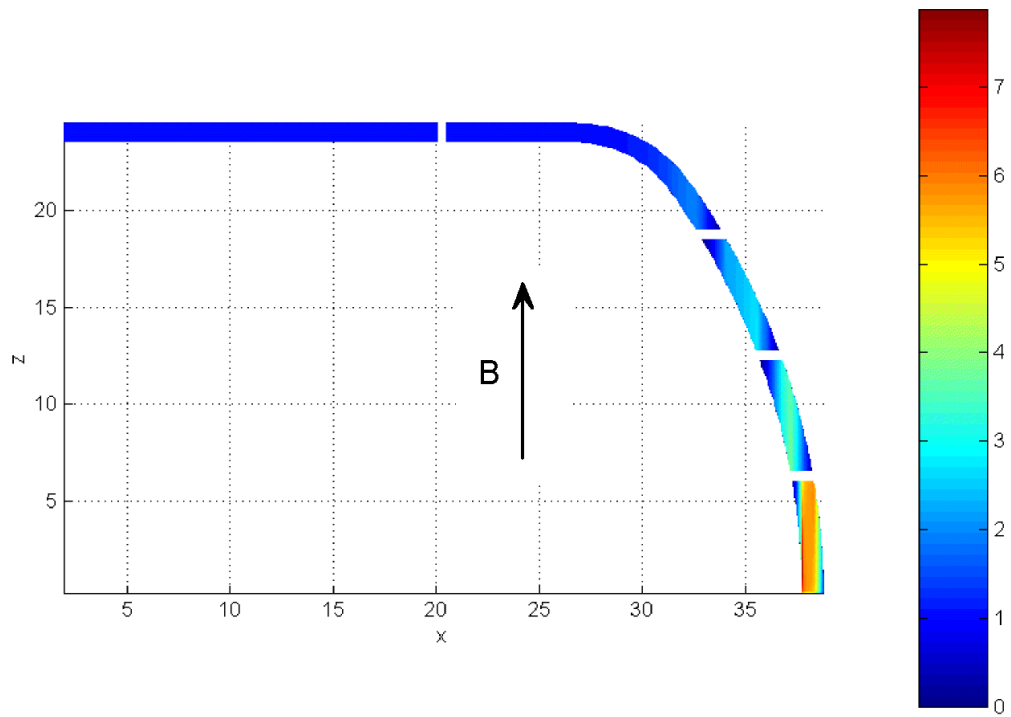


Figure 18: Colored contours of velocity in sub channels D1-D5 for an overview. Equal pressure drops in all sub channels.

3.3 Central duct

Finally we consider the flow in the central duct. A typical length scale here would be the half width measured along field lines. However, in order to have results which are comparable with data obtained before, we keep the gap width as a measure for the length scale. The profile of a fully established axial flow is shown in Fig. 19. The core velocity is uniform almost everywhere, but reduces to smaller values for $x < -20.75$. For $x > 26.625$ the core velocity decreases and drops to zero finally at the point, where the wall is tangential to the magnetic field. along all walls we observe the thin viscous Hartmann layers. The nondimensional pressure drop for this duct is really small, $\nabla p_c = 9.1 \cdot 10^{-5}$. This corresponds in physical units to $\nabla p_c = 0.104 \text{ kPa} / \text{m}$.

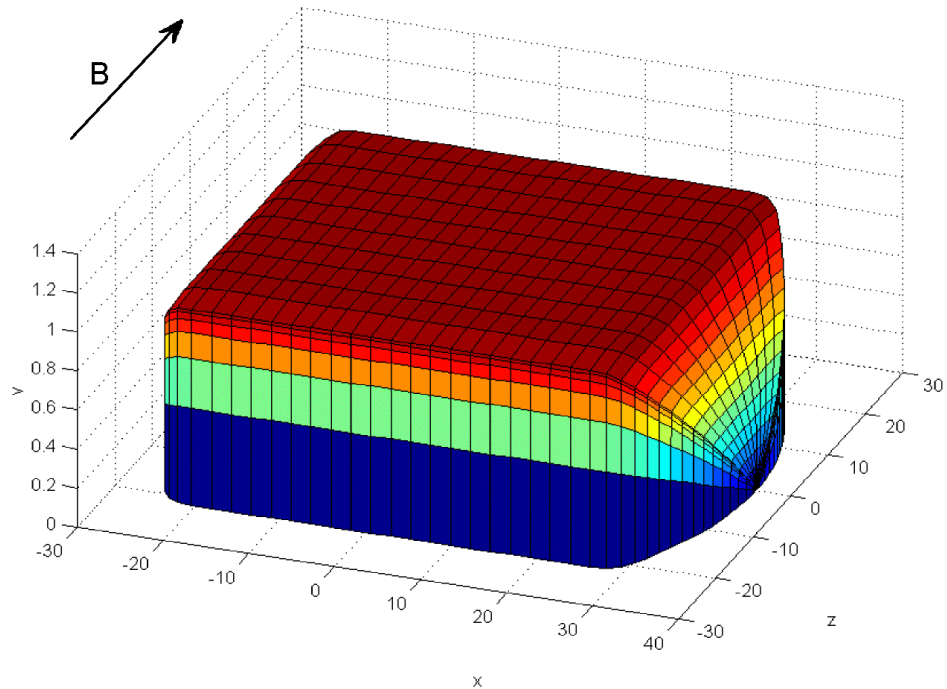


Figure 19: Perspective view on the velocity profile in the central duct.

4 Results for design 2

4.1 Annular sub channels

For various reasons a second design of the plasma facing geometry has been considered. In this design the front part is built as a semi-circle as shown in Figs. 20 and 21. The gap width remains at $L = 0.004$ m. Due to the curvature of the geometry the uniform heat flux $\mathbf{q} = -q \hat{\mathbf{x}}$ creates a surface normal heat flux $\mathbf{q} \cdot \mathbf{n} = q \cos \varphi$. Consequently the high velocity $v = 4.5$ m/s is required only near $\varphi = 0$ for heat removal. For larger values of φ the velocity may decrease as the surface normal heat flux. For safe operations we assume, however, that the average velocity in duct D5 is not smaller than $v_0 = 1.5$ m/s. The spacing between individual sub-ducts is chosen now in such a way that the velocity near the first wall varies similarly as the surface heat flux from the value of roughly 4.5 m/s to the value of 1.5 m/s. This leads to a shorter toroidal length for the ducts D1 and D2. It is not possible to affect the velocity profiles in ducts D3 – D5 since in these ducts the determining length is the spacing, measured along field lines, between the inner and outer cylinder and not primarily the length of the sub-domains. Therefore, for the chosen gap width, it is not possible to achieve the $\cos \varphi$ profile exactly. If it is really required to satisfy such a constraint, it would be possible to do so by introducing a gap width which varies along φ in the proper way.

We assume again fully developed conditions, i.e. the variations of cross sections are very small along the length of the channels.

The velocity profiles in the individual sub channels are qualitatively as for the design 1 and skipped here. We show immediately the results for the whole annular region. Results are presented for the case when all ducts are connected to the same "pressure reservoir". The influence on the flow rates is shown in Tab. 4 and in Fig. 22.

Table 4: Average velocities in sub channels for equal pressure drop (design 2)

Duct	∇p	v_0	∇p (MPa / m)	v_0 (m / s)
D1	0.0036	3.103	0.0567	4.65
D2	0.0036	2.292	0.0567	3.44
D3	0.0036	1.989	0.0567	2.98
D4	0.0036	1.343	0.0567	2.01
D5	0.0036	1.000	0.0567	1.50
D6	0.0036	0.947	0.0567	1.42

We can now take profit from the fact that the average velocity increases by a factor of 3 when we approach the center of the first wall in the blanket module as now the surface heat flux increases in a very similar way. This may reduce the MHD pressure gradient for the semi-circular geometry by a factor of 3 in comparison with that in design 1. Nevertheless, we must keep in mind that regions of reduced velocities near the points A are still present.

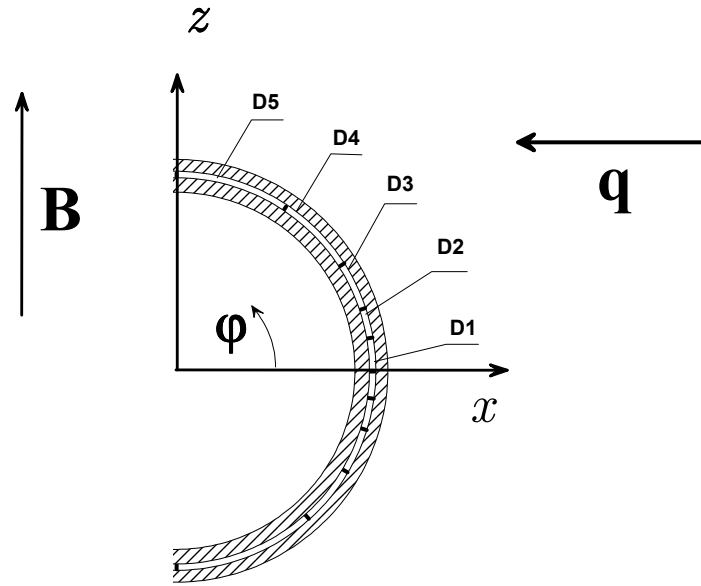


Figure 21: Sketch of the first wall region for design 2. Coordinates and sub channels.

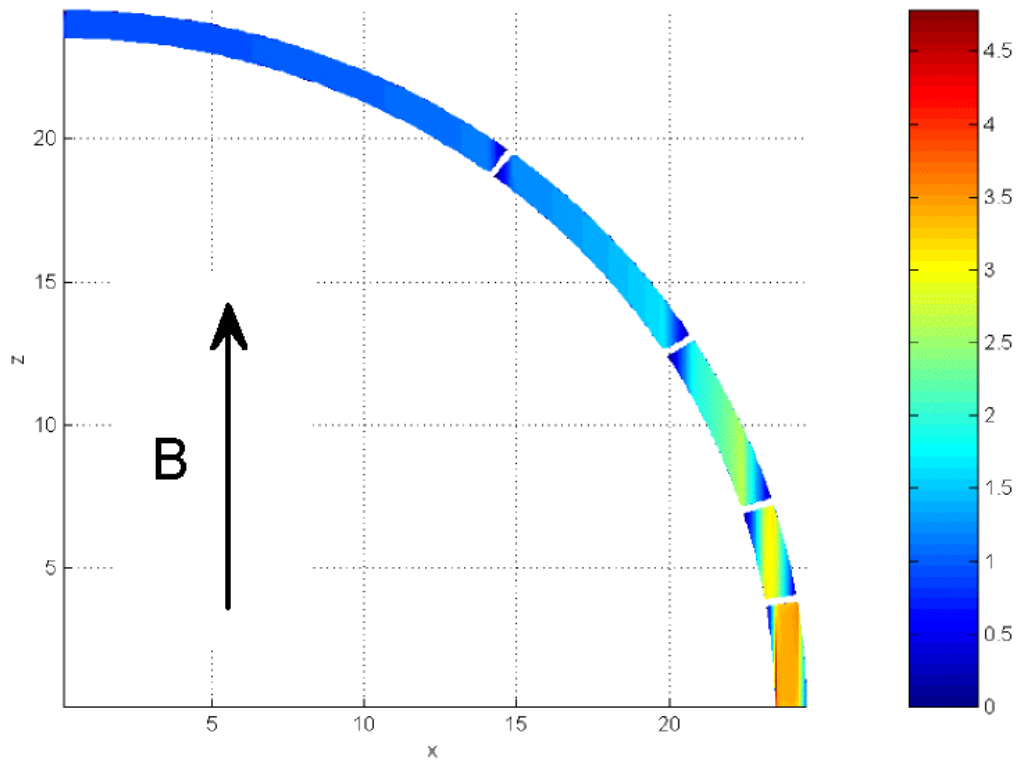


Figure 22: Colored contours of velocity in sub channels D1 – D6 for an overview. Equal pressure drops in all sub channels.

5 Conclusions

The fully developed magnetohydrodynamic pressure drop in a typical geometry of the European SCLL blanket has been evaluated, assuming a uniform transverse magnetic field. The analysis has been performed using a code that solves by asymptotic and numeric techniques the three-dimensional governing equations for conservation of momentum, mass, and charge, and Ohm's law for strong, externally applied magnetic fields. The calculations show that the design 2 with the circular type of geometry has better MHD performance than the design 1. The pressure gradient in the annular ducts made by insulating walls is about $\nabla p = 0.0567$ MPa/m at velocities as foreseen in the annular gap $v_0 = 1.5 - 4.5$ m/s. The pressure drop in the central duct is negligible in comparison with the pressure drop in the annular region. The total pressure drop is mainly created in the annular gap. Its values seem to be on acceptable magnitude. Over the total length $L_t = 7.8$ m of the outboard blanket the pressure drops by $\Delta p = 0.44$ MPa. These results have been obtained assuming a uniform magnetic field of 4 T for the outboard blanket. The top blanket is positioned in a region where the magnetic field is roughly estimated to $B_0 = 6$ T while at the inboard blanket we have $B_0 = 8$ T. If the geometry for the top and the inboard blanket is the same we can simply estimate the pressure drop there by using the linear dependence of the MHD pressure drop on the magnetic field for a reasonable extrapolation. This yields pressure gradients $\nabla p = 0.085$ MPa/m and $\nabla p = 0.11$ MPa/m and pressure drops $\Delta p = 0.19$ MPa and $\Delta p = 0.85$ MPa for the top and for the inboard blanket, respectively.

It is found that the core velocity profiles along the first wall exhibit a decrease when approaching the points A at the walls dividing the annular gap into a number of sub channels. This "periodic" velocity distribution may have a negative influence on heat transfer. Such flows create non-uniform temperature distributions along the first wall with resulting thermally induced stresses. It is found also that the mean velocity in the annular sub channels changes along the first wall, when all the channels are connected to the same pressure reservoirs. This latter effect is used by choosing the appropriate toroidal extension of the channels in order to achieve the flow rates required for heat removal from the first wall. The toroidal extensions of ducts in the rear gap should be held smaller than those along the first wall in order to avoid that a large fraction of the flow bypasses the first wall thorough the sub channels in the back of the blanket box.

Three-dimensional effects have not been taken into account so far. If we consider the blanket in closer detail we see that the cross sections change slowly along the poloidal height. The magnitude of the toroidal field does also show spatial variations. Both effects should be taken into account in future studies. Additional MHD pressure drop is expected also near the blanket ends, where the flow turns.

From the preliminary drawings of the blanket it is not obvious how the liquid metal is supplied to the blankets. If this is done through relatively thin pipes there exists the possibility that the pressure drop there exceeds the one obtained for the blanket, especially if there is a number of bends in the magnetic field region. It is therefore recommended to make the supplying pipes as short as possible. Finally it should be mentioned that each penetrations through the fringing magnetic field causes an additional irreversible pressure drop.

References

- Bühler, L.: 1994, Magnetohydrodynamic flows in arbitrary geometries in strong, nonuniform magnetic fields.- A numerical code for the design of fusion reactor blankets, *Fusion Technology* **27**, 3–24.
- Bühler, L.: 1999, Poloidal MHD flow in the European TAURO blanket concept, *Technical Report FZKA 6384*, Forschungszentrum Karlsruhe.
- Bühler, L.: 2001, Fully developed MHD flow in the European TAURO concept for a nuclear fusion blanket, *Magnetohydrodynamics* **37**(1-2), 127–134.
- Enderlé, R., Giancarli, L., Golfier, H., Poitevin, Y. and Szczepanski, J.: 2002, SCLL reactor design. Communicated by L. Giancarli, May 2002.
- Giancarli, L., Bühler, L., U. Fischer and, H. G., Maisonnier, D., Poitevin, Y., Szczepanski, J. and Ward, D.: 2003, In-vessel component designs for a self-cooled lithium-lead fusion reactor, *Fusion Engineering and Design to be published*, Proceedings of the 22nd Symposium on Fusion Technology, Sept. 9–13, 2002, Helsinki, Finland.
- Jauch, U., Karcher, V., Schulz, B. and Haase, G.: 1986, Thermophysical properties in the system Li-Pb, *Technical Report KfK 4144*, Kernforschungszentrum Karlsruhe.
- Malang, S. and Tillack, M. S.: 1995, Development of self-cooled liquid metal breeder blankets, *Technical Report FZKA 5581*, Forschungszentrum Karlsruhe.
- Moreau, R.: 1990, *Magnetohydrodynamics*, Kluwer Academic Publisher.
- Müller, U. and Bühler, L.: 2001, *Magneto-fluid dynamics in Channels and Containers*, Springer, Wien, New York. ISBN 3-540-41253-0.